energies

MDPI

Article

Research on the Hybrid Wind–Solar–Energy Storage AC/DC Microgrid System and Its Stability during Smooth State Transitions

Qiushuo Li *, Xinwei Dong, Mengru Yan, Zhao Cheng and Yu Wang

School of Electrical and Engineering, China University of Mining and Technology, Xuzhou 221116, China; 4614@cumt.edu.cn (X.D.); ts22230173p31@cumt.edu.cn (M.Y.); ts22230097p31@cumt.edu.cn (Z.C.); ts22230161p31@cumt.edu.cn (Y.W.)

* Correspondence: ts22230034a31@cumt.edu.cn; Tel.: +86-113852155620

Abstract: The hybrid AC/DC microgrid is an independent and controllable energy system that connects various types of distributed power sources, energy storage, and loads. It offers advantages such as a high power quality, flexibility, and cost effectiveness. The operation states of the microgrid primarily include grid-connected and islanded modes. The smooth switching between these two states is a key technology for ensuring the flexible and efficient operation of the microgrid. In this paper, the typical structure of an AC–DC hybrid microgrid and its coordination control strategy are introduced, and an improved microgrid model is proposed. Secondly, an adaptive current–voltage–frequency integrated control method based on signal compensation is proposed to solve the impulse current and voltage generated during the switching between a grid-connected state and an off-grid state. Finally, in response to unplanned grid-connected scenarios, an improved pre-synchronization control strategy based on BP neural networks is introduced to rapidly restore stable operation. The proposed control strategies enhanced the steady-state and transient stability of the hybrid wind–solar–energy storage AC/DC microgrid, achieving seamless grid-connected and islanded transitions without disturbances. The simulation and experimental results validated the correctness and effectiveness of the proposed theories.

Keywords: hybrid AC/DC microgrid; smooth switching between grid-connected and islanded modes; control strategies; BP neural networks algorithm; stability control

Citation: Li, Q.; Dong, X.; Yan, M.; Cheng, Z.; Wang, Y. Research on the Hybrid Wind–Solar–Energy Storage AC/DC Microgrid System and Its Stability during Smooth State Transitions. *Energies* **2023**, *16*, 7930. https://doi.org/10.3390/en16247930

Academic Editors: Il-Yop Chung and Seon-Ju Ahn

Received: 28 October 2023
Revised: 24 November 2023
Accepted: 5 December 2023
Published: 6 December 2023

1. Introduction

In recent years, with the aggravation of resource scarcity and environmental pollution issues, the proportion of distributed generation (DG) represented by photovoltaic and wind power in the power grid is increasing, which brings many advantages such as protecting the environment, reducing power generation costs, and improving resource utilization. It also leads to intermittent output fluctuation, power quality decline, and many other hazards. Microgrids, especially hybrid AC/DC microgrids, have emerged as intelligent micro-power systems that maximize the advantages of DG. They integrate various types of distributed energy sources, energy storage systems, loads, controls, and various protection measures [1]. Its unique bidirectional AC/DC converter, which enables smooth power flow between AC and DC sub-microgrids, reduces the power conversion process and improves power supply reliability [2]. Presently, hybrid AC/DC microgrids are predominantly solar-storage-based and wind–solar-storage-based. However, at the same time, because of the intermittent photovoltaic and wind resources, they have a certain instability.

Hybrid AC/DC microgrids operate in two basic states: grid-connected and islanded. During state transitions, the system structure will change, leading to voltage and frequency variations, and various issues like current surges, voltage fluctuations, and frequency mutation. This can jeopardize the stable operation of the microgrid and even affect the

safety of the main grid. Therefore, ensuring the smooth transition between grid-connected and islanded states is essential for improving the microgrid's safety and stability.

Currently, the control strategies for individual AC or DC microgrids during state transitions are relatively mature [3–8], but there are few studies involving both AC and DC microgrids [9]. In order to solve the problem of voltage shock during the switching process, the literature [3] proposed an improved voltage loop controller, which reduces the surge current, but lacks a solution for addressing current and frequency transients. Reference [4] put forward a hybrid control method based on master–slave control, combining droop control in the grid-connected mode and V/f control in the islanded mode. Although this improved the control accuracy, switching between different control methods can cause instability among the related parameters. In order to ensure smooth switching between the operating modes and reduce the impact of transient switching, the literature [5] proposed a new software phase-locked loop (PLL) control, including instantaneous grid phase detection, off-grid phase-locking technology, and a frequency compensation phase pre-synchronization algorithm. However, pure software control has high hardware stability requirements and cannot meet the needs of unplanned grid-connected and islanded transitions. In the literature [10], an improved hybrid voltage and current control mode was proposed to realize smooth switching between inverters and off-grid, but the control mode needed to be changed during the switching process, and there were deviations in the voltage and frequency under the off-grid operation. In addition to improving the voltage and current loop control, pre-synchronous control is also an effective control method for realizing the off-grid state to the grid-connected state. The literature [11] used pre-synchronization control to pre-adjust the output voltage, frequency, and power of the inverter before switching, effectively suppressing the problem of the voltage and current distortion in the traditional switching process. However, due to the functional limitations of the PI controller itself, the phase difference after several cycles was approximately zero after the output of the PI controller, resulting in an insufficient adjustment function.

Based on the above research results, it can be found that the current AC–DC hybrid microgrid lacks a microgrid model that can solve its steady-state instability in the process of stable operation. There is a lack of control methods that can solve the transient fluctuation of the AC–DC hybrid microgrid in the process of on-grid and off-grid state switching.

On this basis, this paper presents an improved model of a wind–solar storage hybrid AC–DC microgrid based on a doubly-fed induction generator (DFIG), along with control methods for smooth transitions between the grid-connected and islanded states, ensuring transient and steady-state stability. The structure of this paper is as follows. In Section 2, the typical structure and coordinated control strategy of an AC–DC hybrid microgrid are introduced, and an improved microgrid model is proposed. The active power control and doubly-fed technology of the DFIG are used to actively adjust the output of the generator to reduce the external impact. In Section 3, an adaptive integrated control method based on the signal compensation for the current, voltage, and frequency is introduced to mitigate the impact of transient currents and voltages during state transitions. Morever, this section also addresses unplanned grid-connected scenarios and presents an improved pre-synchronization control strategy based on BP neural networks to resolve the inadequacies of traditional pre-synchronization control. In Section 4 presents the improved wind–wind storage hybrid microgrid model built on the Matlab/Simulink (R2022b) simulation platform, and the accuracy and effectiveness of the impact-free smooth grid-connected and off-grid switching control strategy is verified. Finally, Section 5 provides a summary of the paper and future prospects.

2. Introduction of the Hybrid Wind–Solar–Energy Storage AC/DC Microgrid System

2.1. Typical Topology of the Hybrid Wind–Solar–Energy Storage AC/DC Microgrid System

The hybrid AC/DC microgrid is composed of an AC microgrid, DC microgrid, and bidirectional AC/DC converter. Compared with the traditional DC microgrid and AC microgrid, it has stronger flexibility and includes two sub-microgrids, an AC microgrid and

a DC microgrid, which can not only accept a variety of units, but also provide energy for different types of loads. In the hybrid AC–DC microgrid, the DC power supply and load are connected to the DC bus, and the bidirectional AC/DC converter is used to exchange power with the AC bus, so that the operation control of the AC side can be better carried out and power can flow between the AC microgrid and the DC microgrid, providing power support for the other sub-microgrids. It ensures the power quality during the grid-connected operation, improves energy utilization, and ensures the safe and stable operation of the whole large system. The typical structure of the hybrid AC–DC microgrid is shown in Figure 1, which is also known as a Type I AC–DC hybrid microgrid structure.

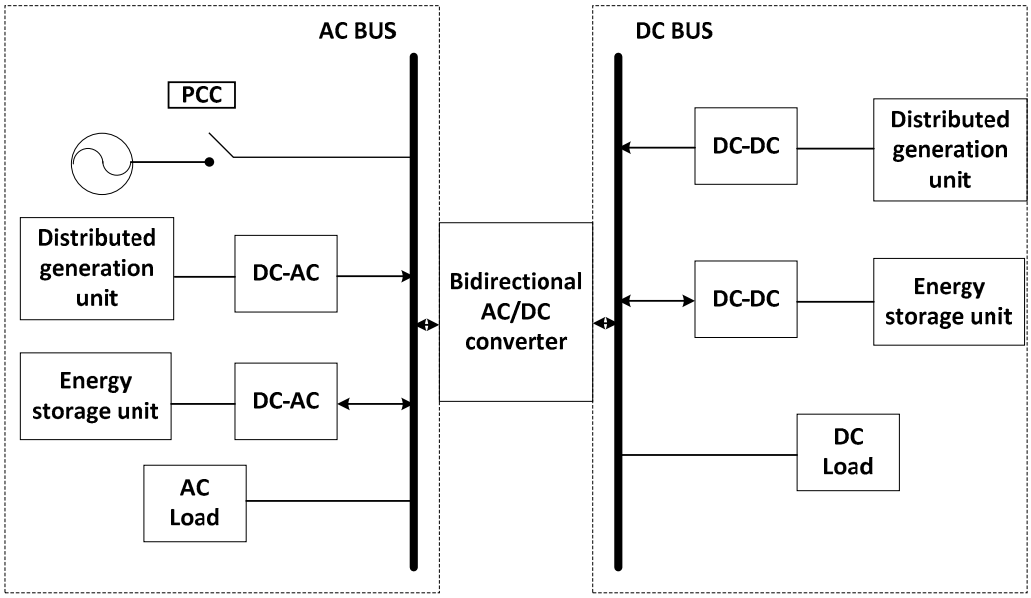

Figure 1. The topology diagram of a Type I hybrid AC/DC microgrid.

The hybrid AC/DC microgrid model used in this paper, namely, the Type I hybrid AC/DC microgrid, has a basic structure in which the point of common coupling (PCC) is connected to both the main grid and the AC/DC microgrid. The AC and DC sub-microgrids are interconnected through bidirectional AC/DC converters. The AC sub-microgrid consists of AC distributed generation units and AC loads, while the DC sub-microgrid comprises DC distributed generation units and DC loads. Due to its connection method and structural characteristics, the Type I hybrid AC/DC microgrid additionally benefits from the main grid's voltage and frequency support for the AC sub-microgrid. This configuration is suitable for microgrids with a significant proportion of AC renewable distributed generation units and AC loads, aligning with the increasing role of renewable energy sources in the power grid. Additionally, it enhances the stability of microgrid system operation [12].

2.2. The General Control Strategy for a Wind–Solar–Energy Storage Hybrid AC/DC Microgrid

The overall control strategy of the microgrid can be divided into master–slave control, peer-to-peer control, and hierarchical control.

(a) Master–Slave Control: The controller of each distributed power generation unit in the microgrid is set up in a subordinate relationship. Typically, the master controller is chosen to be a unit with high inertia and capacity, responsible for providing voltage magnitude and frequency support to the distributed generation units within the microgrid. The slave controllers, benefiting from this support, generally employ direct P/Q control to adjust the power output. This control strategy offers simplicity and flexibility during normal microgrid operation but may face control breakdown during abnormal microgrid operation.

(b) Peer-to-Peer Control: In contrast to master–slave control, peer-to-peer control treats all the units in the microgrid as equals and often employs droop control. All the micro-sources can adjust their power output by varying the frequency and amplitude of their output voltage. However, droop control also has the disadvantage of causing the bus voltage and frequency to drop.

(c) Hierarchical Control: Hierarchical control typically involves a coordinating controller responsible for harmonizing the operation of local distributed energy sources and loads, ensuring the secure and stable operation of the microgrid. To maximize the consumption of distributed energy and ensure the stable operation of the microgrid, a two-times non-differential voltage regulation and a two-times non-differential frequency regulation of the AC sub-microgrid in the local control layer can be achieved. Based on these advantages, the wind–solar–energy storage hybrid AC/DC microgrid proposed in this paper will employ a hierarchical control approach for overall microgrid control.

The bidirectional AC/DC converter plays a crucial role in connecting the AC subnet and the DC subnet and realizing the power flow between the subnets. When there is a power surplus or power deficit in the AC/DC subnetwork, the bidirectional AC/DC converter can work in the rectification or inverter mode to transfer or provide power to another subnetwork. Therefore, researching the control strategy of bidirectional AC/DC converters is of great significance in the steady-state and transient stability studies of hybrid AC–DC microgrids. The traditional control methods of a bidirectional AC/DC converter include V/F control, P/Q control, and droop control.

V/F control [13] means constant voltage and constant frequency control, as shown in Figure 2. When the AC/DC hybrid microgrid operates in the island mode, the AC sub-microgrid loses the support of the large power grid, and the bidirectional AC/DC converter provides constant voltage and frequency support for the bus of the AC sub-microgrid to maintain the stable operation of the AC–DC hybrid microgrid.

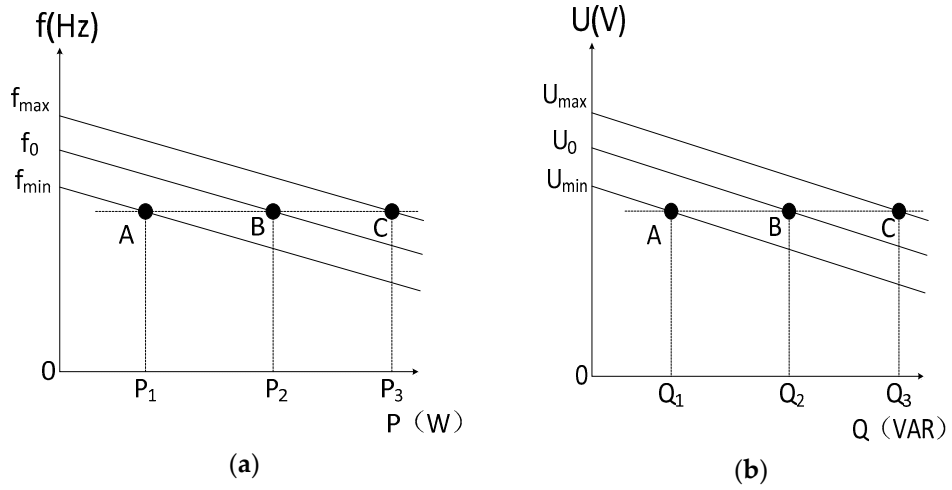

Figure 2. Schematic diagram of V/F control. (**a**) The P-f curve; (**b**) the Q-U curve.

The P/Q control, also known as power balance control [14], is depicted in Figure 3. The voltage of the AC and DC buses is normalized. By using the normalized deviation "n" between the AC and DC bus voltages, the power balance of the hybrid AC–DC microgrid is determined, and the PI controller is used to control $U_{ac} = U_{dc}$. When n > 0, the AC sub-grid provides power support to the DC sub-grid; when n < 0, the DC sub-grid provides power support to the AC sub-grid; and when n = 0, the power of the AC–DC microgrid reaches balance.

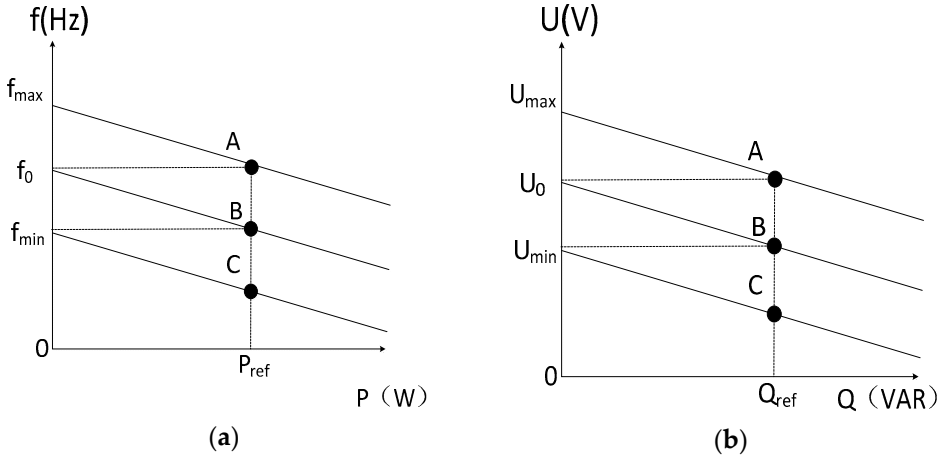

Figure 3. Schematic diagram of P/Q control. (**a**) The P-f curve; (**b**) the Q-U curve.

As shown in Figure 4, the droop control strategy employed in the hybrid AC–DC microgrid is actually a droop control strategy determined by two variables [15], which adjusts the power of distributed generation according to the droop characteristic P-f. Specifically, the transmission power of the bidirectional AC/DC converter is obtained according to the frequency–voltage deviation of the DC sub-grid named $P_{ac} - f_{ac}$ and the frequency–voltage deviation of the AC sub-grid named $P_{dc} - f_{dc}$. When the active power in the microgrid increases and the frequency decreases, the droop controller adjusts the active power of distributed generation based on the droop characteristics. When the reactive power in the microgrid increases and the voltage amplitude decreases, the droop controller adjusts the reactive power based on the droop characteristics. However, during grid-connected and off-grid switching, the frequency of the microgrid fluctuates seriously. Droop control, a control mode guided by frequency power control, has the disadvantage of causing a drop in the bus voltage and frequency, so it is not suitable for grid-connected and off-grid switching.

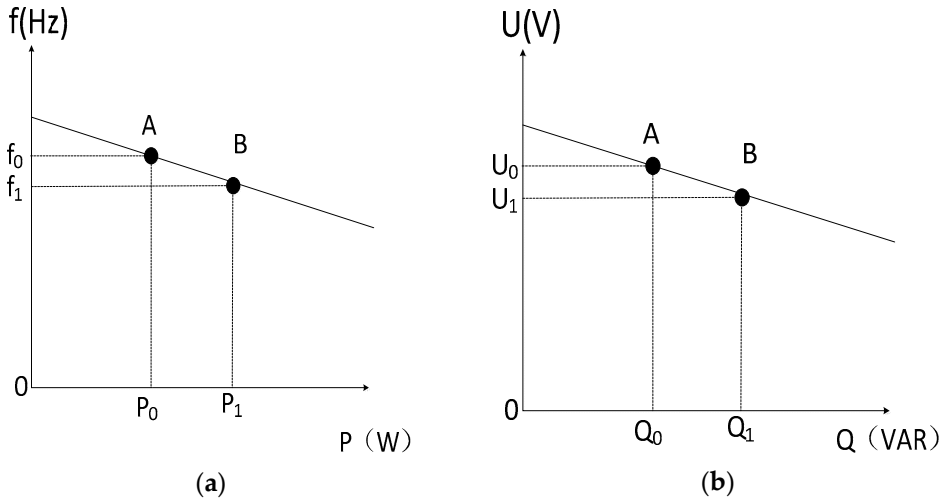

Figure 4. Schematic diagram of droop control. (**a**) The P-f curve; (**b**) the Q-U curve.

Based on the above analysis, the overall control of the wind–wind storage AC–DC hybrid microgrid proposed in this paper adopted the hierarchical control mode. The bidirectional AC/DC converter adopted the P/Q control mode and V/F control mode, and switches the control mode according to the grid-connected and off-grid real-time signals. Specifically, when the microgrid is grid-connected, the bidirectional AC/DC converter operates in P/Q control mode. When the microgrid is in an off-grid state, the bidirectional

AC/DC converter switches to the V/F control mode. The selection of the control mode maximizes the stability of the steady-state and transient operation of the microgrid.

2.3. Improved Hybrid Wind–Solar–Energy Storage AC/DC Microgrid System Model

In order to achieve a greater degree of clean energy utilization, this paper selected the Type I hybrid AC/DC microgrid and made improvements to its specific topology, as illustrated in Figure 5 The enhanced hybrid AC/DC microgrid comprises a DC sub-grid, an AC sub-grid, and a control center.

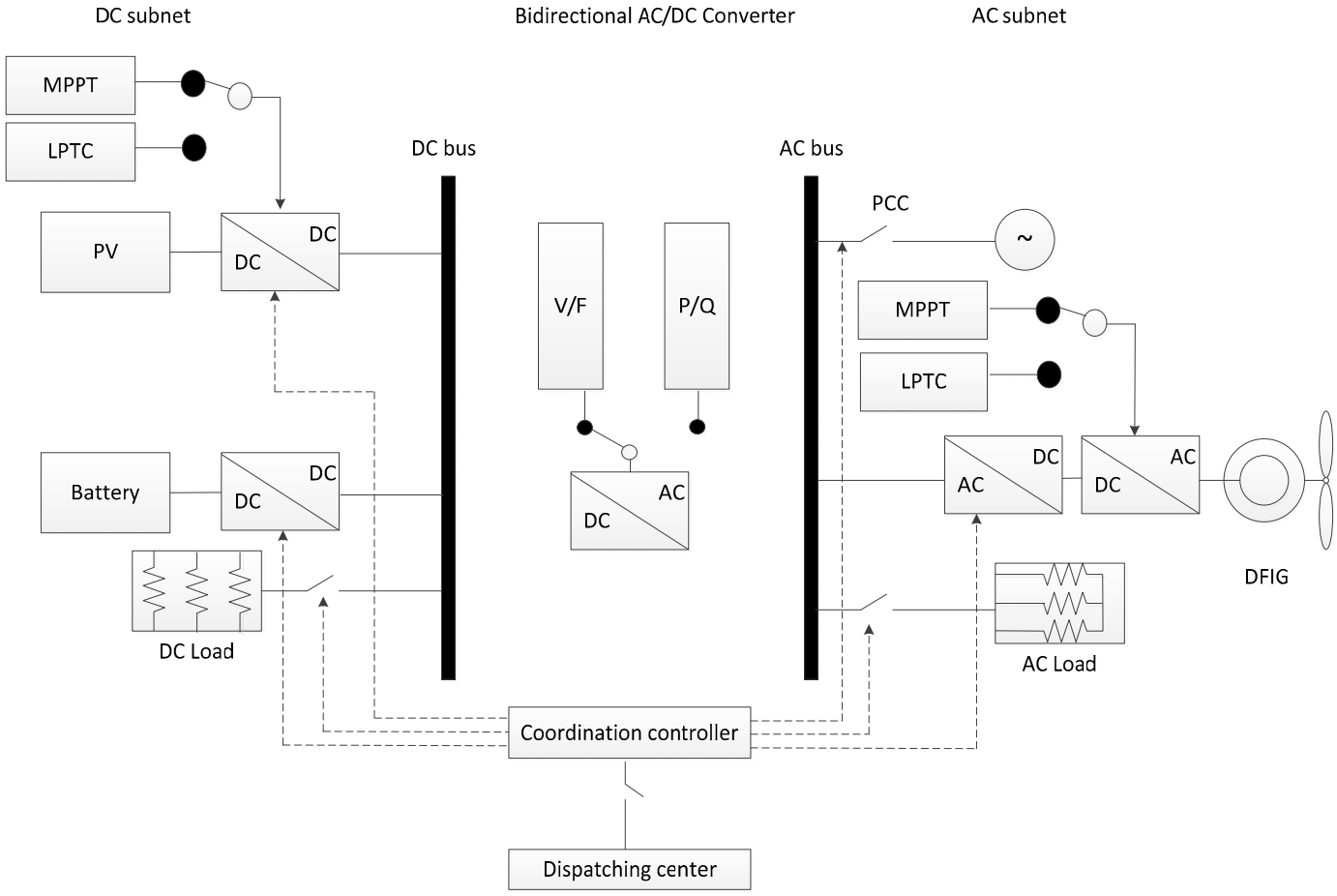

Figure 5. The topology diagram of the improved hybrid wind–solar–energy storage AC/DC microgrid system.

The DC sub-grid consists of photovoltaic generation units, a battery bank, DC loads, power converters, and a DC bus. The photovoltaic generation units and the battery bank are connected in series with power converters and then connected in parallel to the DC bus.

The AC sub-grid includes a DFIG, AC loads, inverters, rectifiers, an AC bus, and a PCC. The DFIG, inverters, and rectifiers are connected in series to the AC bus. The PCC is used to link the main grid and the hybrid AC/DC microgrid, while the AC loads and wind power generation units are connected in parallel to the AC bus.

The control system comprises bidirectional AC/DC converters, a coordinating controller, and a dispatch center. The coordinating controller includes a pre-synchronization controller, a phase-locked loop (PLL), and current–voltage–frequency control loops for stabilizing the relevant parameters of the microgrid.

In order to improve the steady-state stability of the system, the traditional simple wind power module was modified into a DFIG. As shown in Figure 6, the DFIG employs a vector control method, where the q-axis component (i_q) of the rotor current controls active

power, and the d-axis component (i_d) controls reactive power, achieving decoupled control of active and reactive power. The DFIG utilizes fundamental control modes, including maximum power point tracking (MPPT) and load power tracking control (LPTC), and issues different current reference commands (i_{qref}, i_{dref}) to control the real-time active and reactive power output. Due to its advantages in the structure and control mode, the DFIG has partial power transfer capability. When the power grid fails or sudden load fluctuation occurs, the DFIG can provide additional reactive power by adjusting the rotor speed and magnetic field to reduce the risk of power failure [16].

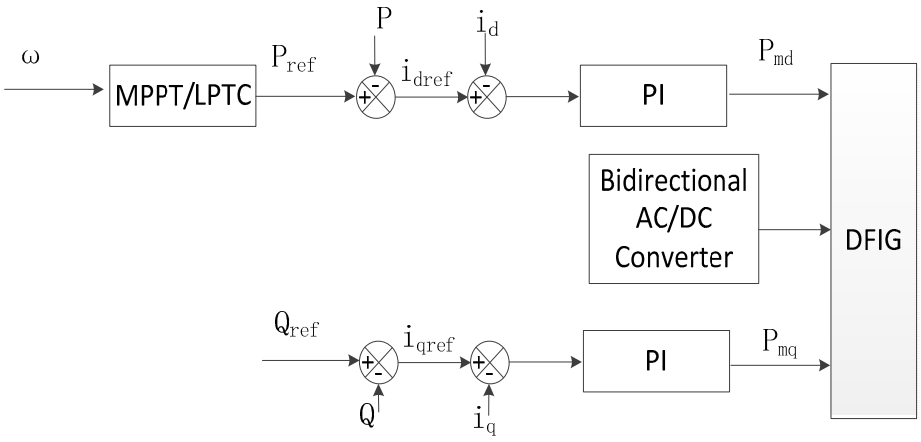

Figure 6. The block diagram of the DFIG.

3. Smooth Switching Control Strategy of the Hybrid Wind–Solar–Energy Storage AC/DC Microgrid System in Grid-Connected and Off-Grid States

In order to achieve smooth transitions between the grid-connected and islanded operation modes of the microgrid and enhance its transient stability, it was necessary to devise a rational control logic. Based on the hierarchical control strategy of microgrids, a set of state switch control logic was designed in this paper, which included two components:

(a) An adaptive integrated control method for the current, voltage, and frequency based on signal compensation.
(b) An improved pre-synchronization control strategy based on a BP neural network.

3.1. The Adaptive Integrated Control Method for the Current, Voltage, and Frequency Based on Signal Compensation

When the AC/DC hybrid microgrid switches between the on-grid state and off-grid state, the control mode of the bidirectional AC/DC converters toggles between the P/Q control and V/F control modes. However, with sudden changes in the outer loop, the voltage and current of the PCC will produce shock and large overshoot, and the frequency will have a large fluctuation, which pose a threat to the safe operation of other renewable energy units and the hybrid AC/DC microgrid.

The voltage loop of the microgrid is a control component within the microgrid system responsible for controlling and maintaining the internal voltage stability. It monitors the voltage level within the microgrid and takes necessary control measures to keep the voltage within an appropriate range. If the voltage inside the microgrid deviates from the set standards or safety levels, the voltage loop employs control strategies such as adjusting the output of the distributed energy resources or scheduling energy storage devices to ensure voltage restoration to normal levels. Similar to the voltage loop, the current loop and frequency loop are utilized to maintain the stability of the current and frequency within the microgrid system, respectively.

This paper adopted an adaptive integrated control method based on signal compensation, as depicted in Figure 7, which included a current loop, voltage loop, and frequency loop, all of which were interconnected and mutually compensated within the three loops.

In this figure, "dq" represents the coordinate transformation section, with "d" and "q" denoting the dq-axis component of the control quantity, respectively, and the subscript "ref" represents the reference value of the control quantity. The switches in the current loop and the voltage loop are configured similarly, where switch state 1 corresponds to the grid-connected state of the microgrid and switch state 2 corresponds to the off-grid state of the microgrid.

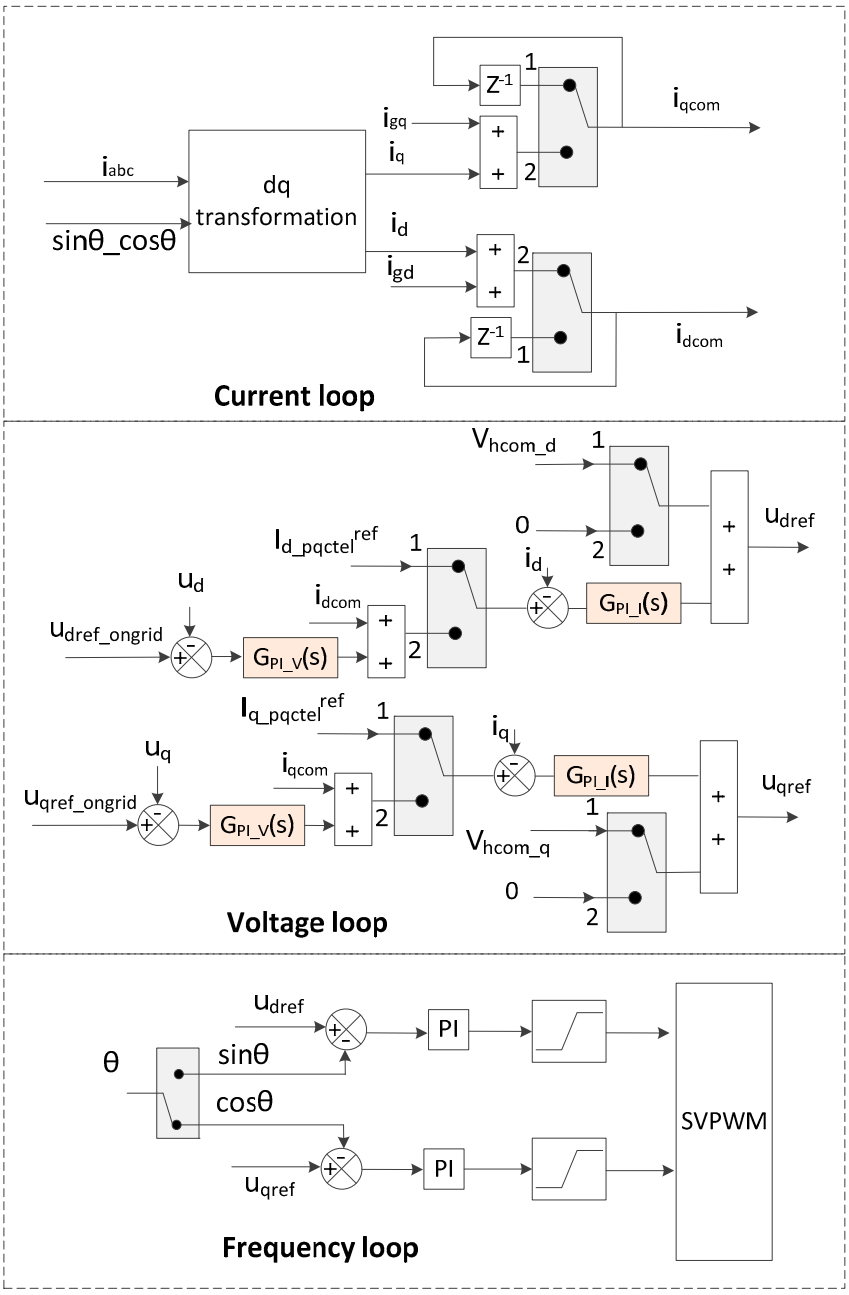

Figure 7. Structure diagram of the signal compensation-based adaptive integrated control method for the current, voltage, and frequency.

In the current loop, during the grid-connected state, the input was the three-phase current signal of the bus. After passing through the dq transformer, it produced separate current signals for the d-axis I_d and q-axis I_q. These signals, first added to the grid current signal I_{gd} and I_{gq}, and then changed to I_{dcom} and I_{qcom} after being adjusted by the PI controller, became the input signal for the voltage outer loop. In the off-grid state, in order to maintain the stable operation of the system, a delay was applied to I_{dcom} and I_{qcom}, so

that the current signal in the off-grid state remains the current value in the grid-connected state until the system is stable.

In the voltage loop during the grid-connected state, the difference between the external reference currents $I_{d\_pqctel^{ref}}$ and $I_{q\_pqctel^{ref}}$ on the d and q axes and the internal current signals I_d and I_q on the d and q axes was taken. This difference was then transformed into voltage signals through the current transformation function $G_{PI\_I}(s)$. Finally, along with the constant voltage reference values V_{hcom_d} and V_{hcom_q} on the d and q axes, it served as the input signals to obtain the output values U_{dref} and U_{qref} of the voltage loop. During the islanded state, the voltage loop underwent a more complex signal processing procedure. The real-time voltage signals U_d and U_q on the d and q axes were compared to the reference voltages U_{dref_ongrid} and U_{qref_ongrid} during the grid-connected operation, resulting in differences. These differences were then transformed into current signals through the voltage transformation function $G_{PI\_V}(s)$. After combining with the current signals I_{dcom} and I_{qcom} from the current loop, the calculated current values were obtained. The differences between these calculated current values and the current signals I_d and I_q on the d and q axes were then transformed into voltage signals through the current transformation function $G_{PI\_I}(s)$. Simultaneously, the voltage reference values were set to zero, directly yielding the output values U_{dref} and U_{qref} of the voltage loop.

In the frequency loop, the input was the voltage phase angle signal, which was transformed into a frequency signal. This frequency signal was then combined and transformed with the output signal of the voltage outer loop, resulting in U_α and U_β. These, along with the DC voltage U_{dc} output from the DC subnet, served as the input signals for the space vector pulse width modulation (SVPWM) inverter. Through mutual signal compensation, this approach more accurately maintained the voltage, current, and frequency stability within the microgrid, enhancing the reliability and power quality of the microgrid.

In the voltage outer loop, when switch = 1, the microgrid was in the grid-connected mode, the output voltage values were V_{Hcom_d1} and V_{Hcom_q1}, and the output current values were i_{dref1} and i_{qref1}. When switch = 2, it was in the islanded mode, the output voltage values were V_{Hcom_d2} and V_{Hcom_q2}, and the output current values are i_{dref2} and i_{qref2}. To avoid voltage deviations and current impacts during the transition between the grid-connected and islanded states, the voltage loop was improved by incorporating current feedback information. In the grid-connected mode, the values were set to $i_{dref2} = 0$, $i_{qref2} = 0$, $V_{Hcom\_d2} = 0$, and $V_{Hcom\_q2} = 0$, and the integral initial value in the PI controller always tracked i_d. At the moment of switching to the islanded mode, the current reference value compensation was introduced and i_d was assigned to the integral initial value, causing it to start changing from the i_d point at the switching moment. This ensured that the output of the voltage loop remained unchanged at the switching moment. Finally, the compensated current reference value was transformed through the G(s) function, superimposed with V_{Hcom_d} and V_{Hcom_q}, and input into the dq transformation. This completed the current superimposition for the voltage loop input value, with the compensation equation as follows.

$$\begin{cases} i_{dref} = i_{dref1} + i_{dref2} \\ i_{qref} = i_{qref1} + i_{qref2} \end{cases} \tag{1}$$

It was assumed that the output power of the bidirectional AC/DC converter was P_{ref2} and Q_{ref2} during the off-grid operation and P_{ref1} and Q_{ref1} during the grid-connected operation, with the objective of making $P_{ref1} = P_{ref2}$ and $Q_{ref1} = Q_{ref2}$, resulting in $i_{dref1} = i_{dref2}$ and $i_{qref1} = i_{qref2}$. This approach followed the provided P_{ref} and Q_{ref}, thereby reducing current disturbances to the microgrid and the main grid.

Based on the analysis presented above, the signal compensation-based adaptive integrated control method proposed in this paper offers the following advantages. The AC/DC hybrid microgrid does not need to use any state following device when transferring from grid-connected to off-grid, and the input quantity of the outer loop of the microgrid does not change at the moment of off-grid. Moreover, the change in the control mode during the transition between the grid-connected and islanded operations only affects the outer

loops, without impacting the inner loops. This greatly enhances the microgrid's transient stability and achieves a smooth, non-impactful transition between the grid-connected and islanded modes.

3.2. Improved Pre-Synchronization Control Method Based on a BP Neural Network

When the operation mode of the microgrid is switched directly from off-grid to grid-connected, due to the inconsistency between the PCC point voltage and the voltage amplitude, frequency, and phase angle of the grid, a large impulse current may be generated, which may damage the power electronic devices and cause the system to crash in serious cases. Therefore, pre-synchronization should be added during the transition from an off-grid state to a grid-connected state.

3.2.1. Details of BP Neural Network

This paper proposes an improved pre-synchronization control method based on BP neural networks, as illustrated in Figure 8. The control deviation of the PID controller is reduced by neural network algorithm, and it is applied to the pre-synchronization controller to reduce the difference in the reference voltage between the phase-locked loop and interconnecting converter in the pre-synchronization control method, so as to improve the control effect of the pre-synchronization control method. It can effectively solve the problem that the output of the phase difference after several cycles is approximately zero after the PID controller in the traditional pre-synchronization control method, resulting in an insufficient adjustment function, reducing the impact current caused by different phase and amplitude, and effectively ensuring the smooth switching of the microgrid off-grid connection.

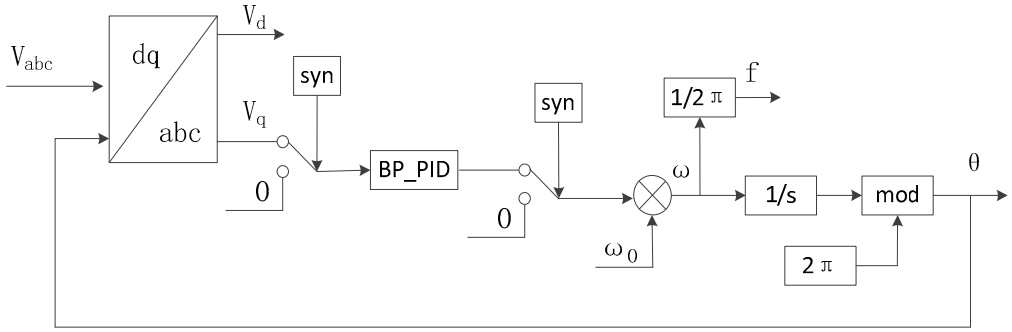

Figure 8. Pre-synchronization control structure diagram.

The specific control block diagram of the PID improved by the BP neural network algorithm proposed in this paper is shown in Figure 9, where Vq is the q-axis component of the real-time AC voltage; Vqref is the q-axis reference voltage; e is the difference between the two; and kp, ki, and kd are the relevant control parameters of the PID controller. The BP neural network algorithm was used to adjust the PID parameters in the PID controller in the pre-synchronization control method in real time. The proportion, integral, and differential gain of the adjusted PID controller can be expressed as follows.

$$\begin{cases} kp = kp0 + \Delta kp \\ ki = ki0 + \Delta ki \\ kd = kd0 + \Delta kd \end{cases} \quad (2)$$

where $kp0$, $ki0$, and $kd0$ are the initial values of the PID parameters, Δkp, Δki, and Δkd are the adjustment quantities generated by the BP neural network algorithm, and kp, ki, and kd are the adjusted PID parameters.

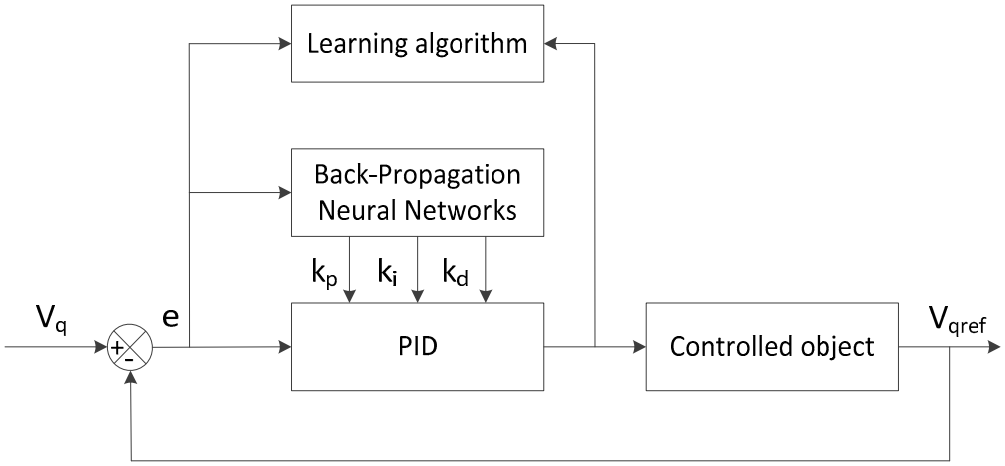

Figure 9. Block diagram of the PID control improved by the BP neural network algorithm.

Let i, j, and l be the number of neurons in the input layer, hidden layer, and output layer, respectively. The input layer of the BP neural network is the q-axis component Vq of the real-time AC voltage, the q-axis reference voltage Vqref, and the error e of both, and the output is the proportional coefficient kp, integral coefficient ki, and differential coefficient kd of the PID controller. The structure of the three-layer BP neural network is shown in Figure 10.

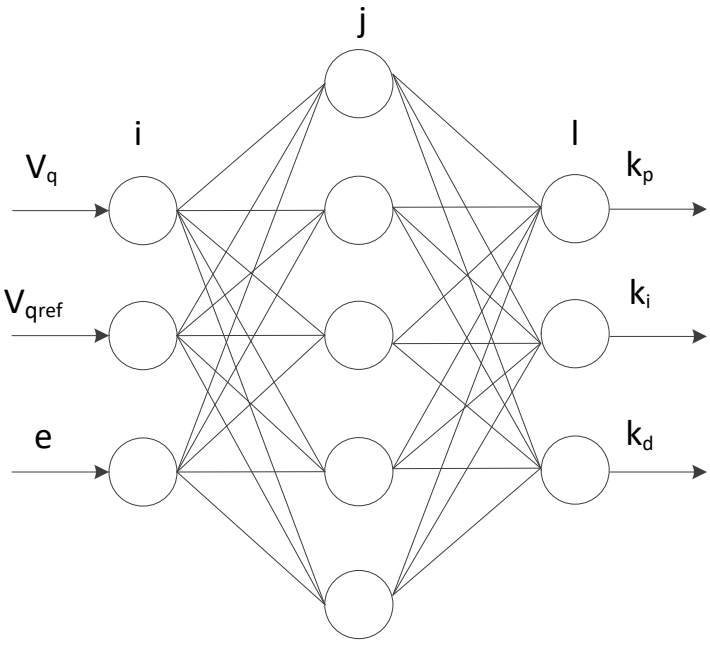

Figure 10. Structure of the BP neural network.

Formula (3) can be obtained by remembering that the JTH neuron of the hidden layer accepts the input layer as a_j.

$$a_j = \sum_{i=1}^{d} V_{ij} x_i \tag{3}$$

Formula (4) can be obtained by remembering that the KTH neuron in the output layer accepts the input from the hidden layer as β_k.

$$\beta_k = \sum_{j=1}^{a} W_{jk} b_j \tag{4}$$

The excitation function selected by the BP neural network is a sigmoid function, and the basic expression of the function is shown as Formula (5).

$$sigmoid(x) = \frac{1}{1+e^{-x}} \tag{5}$$

Then, the output of the neural network, namely the three parameters of the PID controller, can be expressed as Formula (6).

$$Y_k^l = f(\beta_k - \theta_k) \tag{6}$$

The backpropagation of the BP network is based on a gradient descent method to find the optimal solution. Through repeated backpropagation, the weight gradually tends toward the optimal solution by constantly adjusting the parameters, and the weight update follows Formula (7). The learning rate is η, and Formula (8) can be obtained.

$$w + \triangle w \to w \tag{7}$$

$$\triangle w_{jk} = -\eta \frac{\partial E_l}{\partial w_{jk}} \tag{8}$$

Here, from the properties of the activation function, that is Formula (9), by combining Formulas (9) and (10), Formula (11) can be obtained.

$$f(x)' = f(x)[1 - f(x)] \tag{9}$$

$$E_l = \frac{1}{2}\sum_{k=1}^{m}\left(Y_k^l - y_k^l\right)^2 \tag{10}$$

$$\frac{\partial E_l}{\partial w_{jk}} = \frac{\partial E_l}{\partial Y_k^l}\frac{\partial Y_k^l}{\partial \beta_k}\frac{\partial \beta_k}{\partial w_{jk}} \tag{11}$$

From Formula (11) and set b_j, Formula (12) can be obtained.

$$\frac{\partial E_l}{\partial Y_k^l}\frac{\partial Y_k^l}{\partial \beta_k} = g_k \tag{12}$$

$$\frac{\partial \beta_k}{\partial w_{jk}} = b_j \tag{13}$$

The expression for updating the weight of the output layer can be derived from Formula (13).

$$\triangle w_{jk} = -\eta \frac{\partial E_l}{\partial w_{jk}} = \eta g_k b_j = \eta Y_k^l(1 - Y_k^l)(y_k^l - Y_k^l)b_j \tag{14}$$

Once the gradient expression has been obtained, the optimal solution can be found by constantly updating the gradient. For the above formula, where η is the learning rate, the learning rate of the BP neural network algorithm was $\eta = 0.25$, and Y_k^l was the output value of the KTH neuron in the output layer of the neural network. Y_k^l was the result of the training output, i.e., the correct output given by the training set; b_j was the output of the JTH neuron in the hidden layer. The values of Vq and Vqref under stable operation of the system were recorded and sampled. A total of 100 values were selected as the training set, and the other 30 samples were selected as the test set. The weights were updated continuously through the above process until the error was sufficiently small and the learning was stopped. To measure the performance of the model and adjust the parameters of the model, improve the performance was improved by minimizing the loss function.

The smaller the mean square error, the closer the prediction of the model to the true value, and the better the performance of the model.

The mean square error loss function of the actual output and the expected output is shown in Formula (10). After 100 iterations, the loss function of the training set and the test set tended to be stable. At this time, the mean square error loss function E_l of the training set was 0.0706 and the error was small.

3.2.2. Pre-Synchronization Control Method

The Clarke and Park transform was carried out to obtain the d-axis component Vgd and q-axis component Vgq, the deviation signal of the q-axis component was obtained through BP-improved PID adjustment, and the phase angle was finally integrated. Two synchronization signals controlled the start and end times of pre-synchronization to prevent integral saturation and disconnect the PID control. Subsequently, using this phase angle, and the $Vabc$ and $ILabc$ of the microgrid through Pike transformation, Vd, Vq, ILd, and ILq were calculated, achieving synchronization of the microgrid's frequency with the public grid. The relationship is expressed by the following equations.

$$f = \frac{Vq\left(Kp + \frac{Ki}{s}\right) + \omega 0}{2\pi} \tag{15}$$

$$\theta = mod\left[\left(\int \omega dt\right), 2\pi\right] \tag{16}$$

As shown in Figure 11, the pre-adjustment of the microgrid voltage frequency was conducted before the grid connection. When connected to the grid, the voltage frequency of the grid side was f_{01}, corresponding to the rated power P_0. Assuming that the microgrid operated in the islanded mode at point A, there existed a certain deviation between the load power P_{Load} at point A and the rated power P_0. Additionally, the frequency f_A at point A deviated from the grid voltage frequency f_{01}. Before transitioning from the islanded mode to the grid-connected mode, it was necessary to ensure the frequency adjustment while keeping the load power constant. The optimal frequency compensation value was obtained through the BP algorithm, and the operation point at point A, represented by the droop curve f_{01}, shifted upwards to curve f_{02}. At this point, the system's operating point moved from A to B. The working frequency f_B at point B coincided with the grid voltage frequency f_{01} during the grid connection, meeting the pre-synchronization conditions while keeping the power constant.

As shown in Figure 12, the pre-adjustment of the microgrid voltage before the grid connection is depicted. The initial droop curve is represented as V_{01}. When the microgrid operated in the islanded mode at point A, the system's rated voltage was V_{01}, and the reactive power Q_{Load} operated with a deviation from the grid's rated value. To achieve synchronization of the voltage with the grid while maintaining constant reactive power, it was necessary to shift the initial droop curve upwards. The optimal voltage compensation value was obtained through the BP algorithm. This adjustment took place in minimal time, moving the operating point from A to B. At point B, the working voltage V_B was exactly equal to the system's rated voltage V_{01}, achieving pre-synchronization of the voltage amplitude. After the completion of this synchronization process, the grid connection operations could be initiated.

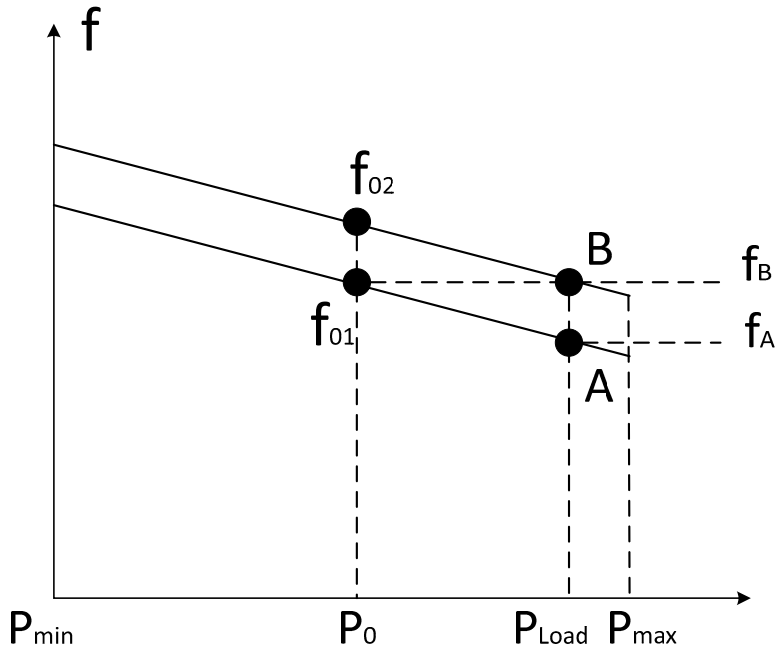

Figure 11. Secondary frequency control.

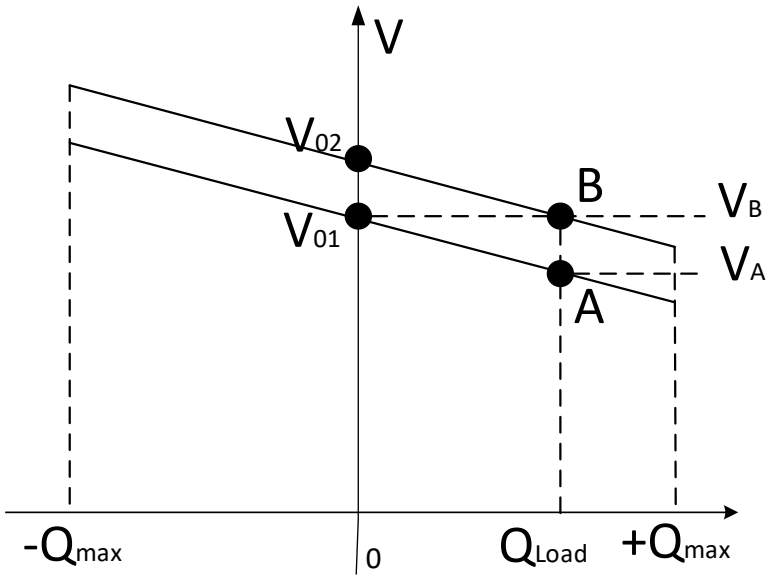

Figure 12. Secondary voltage control.

4. Simulation Results and Analysis

To verify the proposed wind–solar–storage hybrid AC/DC microgrid and its smooth grid connection and disconnection control strategy, an I-type microgrid was constructed, which included a DC microgrid, an AC microgrid, and bidirectional AC/DC converters, as shown in Figure 1. Experimental validation was conducted using the primary parameters listed in Table 1.

The microgrid was controlled to change from the grid-connected mode to the island mode in the first second, and from the island mode to the grid-connected mode in the second. This state transformation was realized by the opening and closing of the PCC points. Specifically, the PCC point switches were set to open and close automatically in the first and second seconds to simulate the unplanned off-grid and grid-connected states. According to the switching of the PCC states described above, the operational modes of the hybrid AC–DC microgrid were as follows. The microgrid was grid-connected within the first second, started islanding from the 1-s mark until the 2-s mark, resumed grid-connected

operation starting at the 2-s mark, and continued until the 3-s mark when the operation concludes. The model was built and simulated in Matlab/Simulink and the fluctuations in bus voltage and current of the hybrid AC–DC microgrid were observed during the 0–3 s period.

Table 1. Parameters of the hybrid wind–solar–energy storage AC/DC microgrid system.

Argument	Parameter Value	Title 3	Parameter Value
Rated voltage of DC bus/V	220	ILC switching frequency/kHz	10
Rated voltage of AC bus/V	380	Alternating current load/kW	20~40
Rated frequency of AC bus/Hz	50	DC load/kW	20~40
Rated power of photovoltaic generation/kW	60	Two-way DC/DC converter inductance/mH	1
Rated wind power/kW	30	Two-way DC/DC converter capacitance/μF	1000
ILC filter inductor/mH	0.8	Boost inductance/mH	1
ILC filter capacitor/μF	82	ILC capacity/kVA	100

First, in the wind–solar–storage hybrid AC/DC microgrid, the wind power generation unit used traditional wind turbines and employed conventional voltage, current, and frequency control loops. The simulation results are shown in Figure 13.

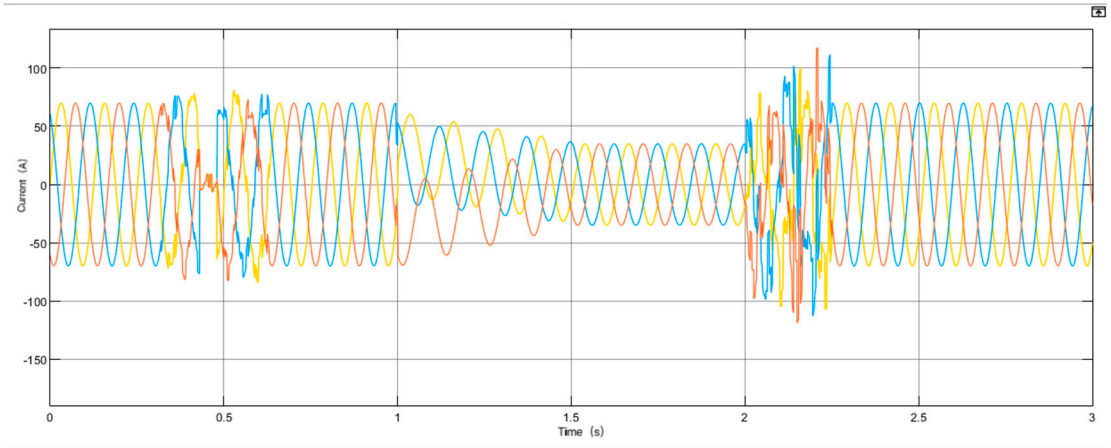

(**a**)

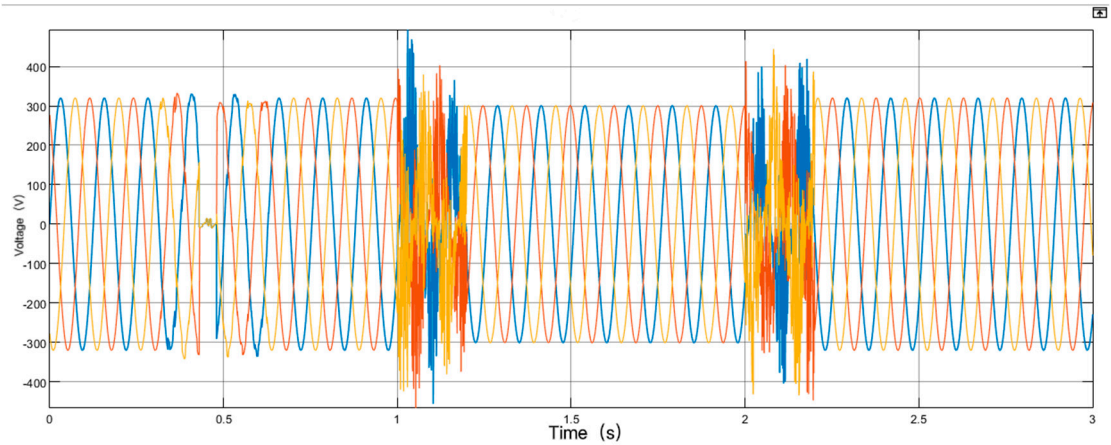

(**b**)

Figure 13. *Cont.*

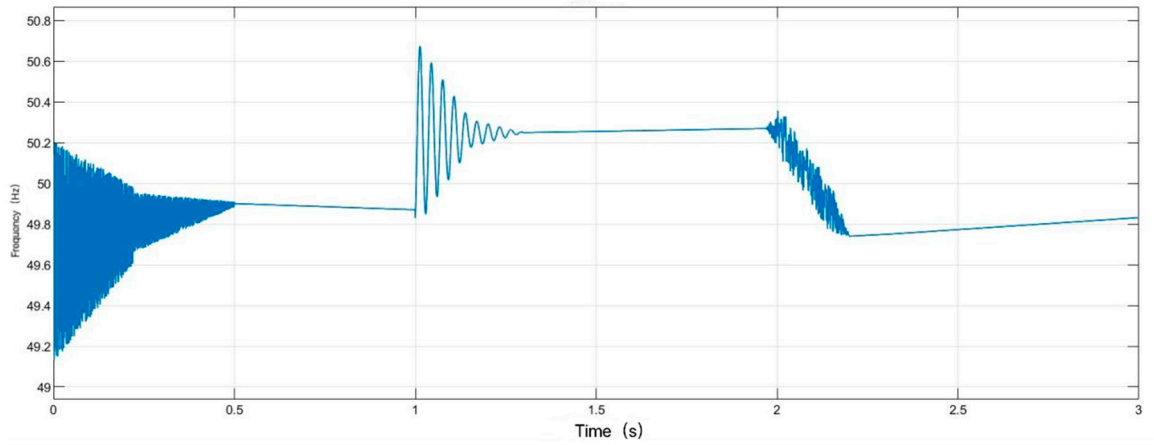

(**c**)

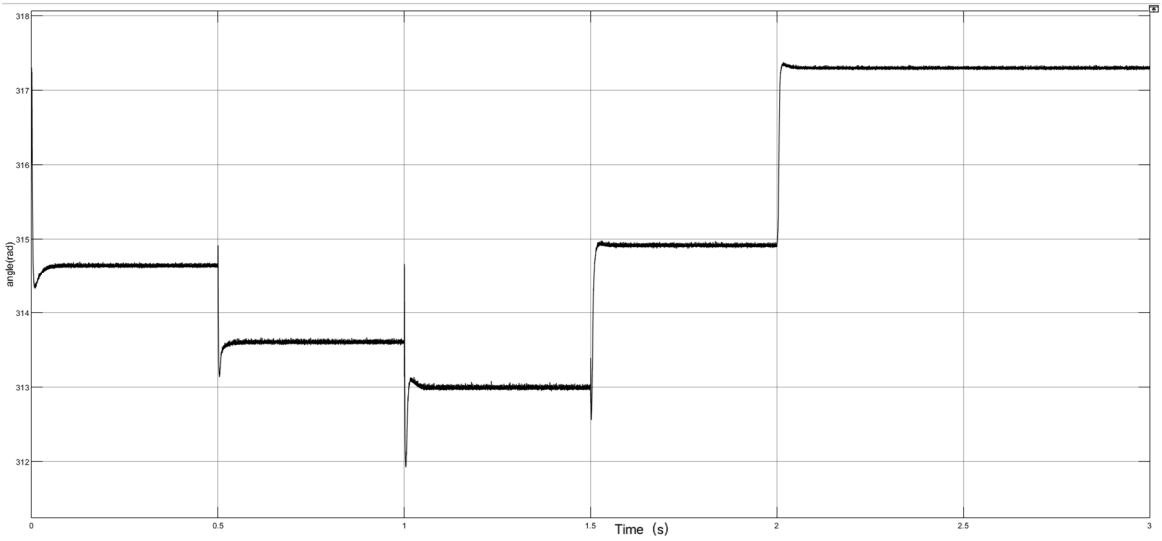

(**d**)

Figure 13. Simulation waveforms of the transition between the islanded mode and grid-connected mode in the hybrid AC/DC microgrid system. (**a**) Current waveform; (**b**) voltage waveform; (**c**) frequency waveform; (**d**) grid angle waveform.

As shown in Figure 13, the steady-state stability of the system was poor. Affected by factors such as wind speed and illumination, voltage and current fluctuations occurred even if the system was in stable operation, and the frequency was not constant. In terms of transient stability, if no additional control strategy was added, the AC/DC hybrid microgrid had huge fluctuations in the voltage, current, and frequency during the on-grid and off-grid switching moments. Specifically, at 1 s, that is, at the moment of the switch from a grid-connected to an off-grid state, due to the sudden loss of voltage support of the large power grid, the microgrid inevitably produced a voltage drop. If not properly controlled, the situation shown in Figure 13 will occur, where the current continues to drop, the current is much smaller than that when the power grid is supported, and the waveform is not a regular three-phase sine wave. The voltage experienced irregular shock fluctuations and could not be recovered in a short time. The frequency fluctuated significantly beyond the range allowed for stability. At 2 s, that is, the moment when the off-grid state was switched to the grid-connected state, the microgrid operated independently and normally in the island state after its own adjustment, but there was a certain gap between the voltage and current between the microgrid and the large power grid. At this time, if there was no pre-adjustment and the difference in the voltage and current parameters between the microgrid

and the large power grid was reduced in advance, the situation shown in Figure 13 will occur. The current and voltage will have serious impact and distortion, and the frequency will also drop sharply until the microgrid is stabilized by the corresponding control after it is connected to the large grid. At the same time, the phase Angle of the grid fluctuated significantly between 312 rad and 317.2 rad, which also indicated the unstable operating state of the system. The above voltage, current, and frequency fluctuations generated at the switching moment were not only detrimental to the stable operation of the microgrid itself, but also excessive impulse voltage and current affected the safe operation of the large power grid. Therefore, appropriate control methods should be taken at the switching moment to make the microgrid quickly enter a stable operation state during state switching, so as to improve the stability of the system and the large power grid.

Figure 14 shows the simulation waveforms of the improved wind–solar battery hybrid AC/DC microgrid and its control strategy during the islanded and grid-connected mode transitions. The use of the DFIG enhanced the system's steady-state stability. Additionally, the integration of the signal compensation-based current–voltage–frequency adaptive control method and the improved pre-synchronization control method based on BP neural networks enabled smooth mode transitions between the islanded and grid-connected states. The fluctuation of the bus voltage and current in the AC/DC hybrid microgrid within 0–3 s was observed again.

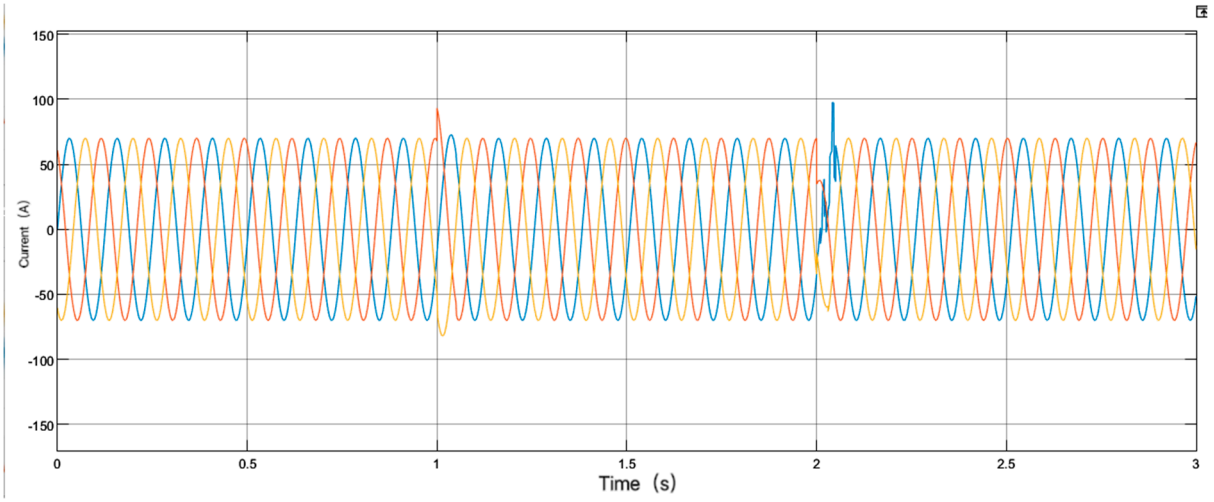

(**a**)

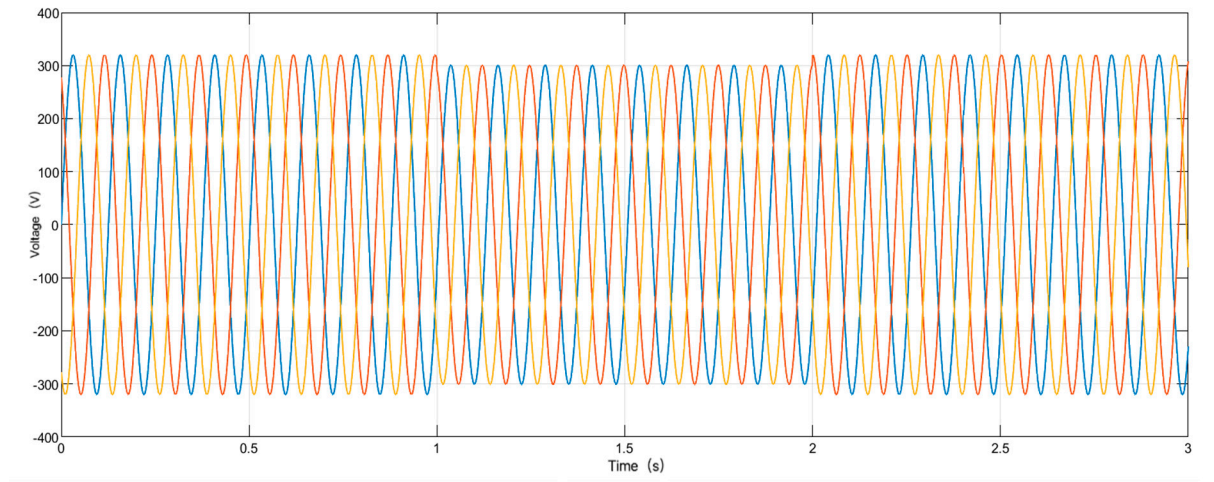

(**b**)

Figure 14. *Cont.*

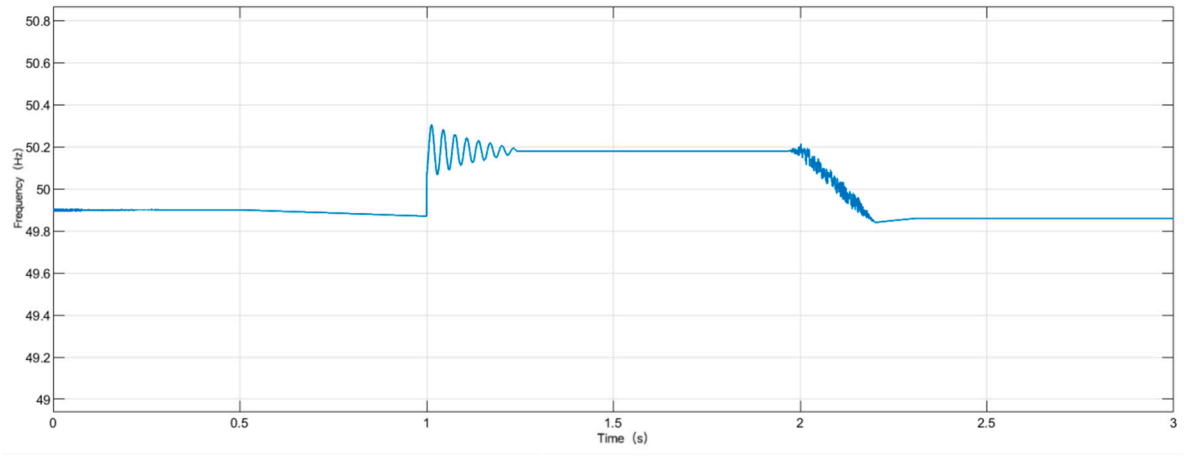

(**c**)

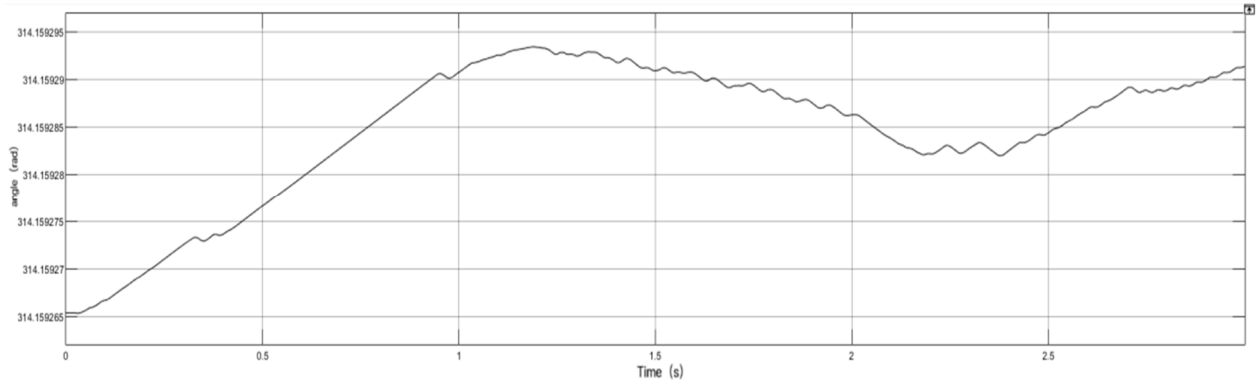

(**d**)

Figure 14. Simulation waveforms of the improved transition between the islanded mode and the grid-connected mode in the hybrid AC/DC microgrid system. (**a**) Current waveform; (**b**) voltage waveform; (**c**) frequency waveform; (**d**) grid angle waveform.

When the microgrid system was connected to the grid at 0–1 s, the output voltage amplitude of the inverter was approx. 320 V, the output current of the inverter was approx. 70 A, the system frequency was 50 Hz, and the system ran stably. At this stage, the photovoltaic power generation system and DFIG were the in MPPT mode, the bidirectional AC/DC converter worked in the V/F control mode, and the energy storage system was charged at a constant power of 20 kW and entered a floating charge state when the battery SOC reached 0.8 to prevent the battery from overcharging and ensure the battery was in the best working conditions.

At 1 s, the microgrid detected an islanded signal and prepared to enter the islanded mode. During this transition, the battery operated in a discharge mode to maintain the microgrid bus voltage, and it reached the switching condition as its output power approached zero, allowing a stable transition to the islanded mode. During this phase, the inverter output current underwent a brief fluctuation but ultimately stabilized back to its initial value of 70 A. The inverter output voltage remained stable at 300 V without voltage spikes. The system output frequency was 49.9 Hz.

At 2 s, the microgrid detected the parallel signal and the microgrid was ready to enter the grid-connected mode. Due to the difference in the voltage, current, and frequency between the microgrid system and the large grid, certain fluctuations occurred when the microgrid system was suddenly connected to the grid. At this time, the pre-synchronization control started. The microgrid started to connect to the grid, stopped the pre-synchronous control, and charged the battery pack until the SOC of the battery pack reached 0.8. The

floating charge was carried out, and the power deficit in the microgrid was provided by the large power grid. When switching from off-grid to grid-connected, the control mode of the photovoltaic power generation system and wind power generation system switched back to the MPPT mode, the bidirectional AC/DC converter switched back to the V/F control mode, and the stable grid-connected state was finally completed. At this stage, the output current of the inverter was stabilized at 70 A after a short drop of 0.1 s, and there was no impulse current. The inverter output voltage was stable at 320 V with no fluctuation. The system output frequency was 50 HZ. At the same time, it can be seen from Figure 14d that during the operation of the microgrid and at the moment of parallel and off-grid switching, the change of the grid angle of the microgrid was less than 0.00003, which indicated that the system was relatively stable during operation.

In summary, the use of the smooth switching control strategy effectively avoided the occurrence of voltage and current spikes during the transitions between the islanded and grid-connected modes. The range of voltage and frequency fluctuations caused by the transitions was within the specified limits ($\Delta f < 0.1 f_N$, $\Delta U < 7\% U_N$), meeting the requirements for the transitions.

5. Conclusions

This paper presented an enhanced model of a wind–solar storage mixed AC/DC microgrid based on a DFIG and its smooth transition control method for grid connection and disconnection.

1. Wind–solar storage mixed AC/DC microgrid based on a DFIG. By using the partial power transfer function of the DFIG, when the power grid failed or sudden load fluctuations occurred, the speed and magnetic field of the DFIG rotor could be adjusted to provide additional reactive power, reduce the risk of power failure, and stabilize the microgrid system.
2. Smooth transition control method for grid connection and disconnection in wind–solar storage mixed AC/DC microgrids. In view of the large fluctuations of the system voltage, current, and frequency caused by the change in the control strategy and PCC point voltage during the state switching process of the microgrid, a current–voltage–frequency adaptive integrated control method based on signal compensation and an improved pre-synchronization control method based on a BP neural network were proposed to effectively improve the transient stability during the state switching process of the microgrid.

The results of this work can be generalized to the grid-connected and off-grid transition control strategies suitable for more complex AC–DC hybrid microgrids, which are being explored by the authors for further research. However, there are still some problems that need further research.

Author Contributions: Conceptualization, Y.W. and Q.L.; methodology, Q.L.; software, Q.L.; validation, Q.L., M.Y. and Z.C.; formal analysis, Q.L.; investigation, Q.L.; resources, Q.L.; data curation, Q.L.; writing—original draft preparation, Q.L.; writing—review and editing, Q.L.; visualization, Q.L.; supervision, X.D. All authors have read and agreed to the published version of the manuscript.

Funding: This research received no external funding.

Data Availability Statement: Data are contained within the article.

Conflicts of Interest: The authors declare no conflict of interest.

References

1. Yang, X.; Su, J.; Lv, Z.; Liu, H.; Li, R. Review on microgrid technology. *Proc. CSEE* **2014**, *1*, 57–70.
2. Zhou, J.H.; Tian, L.G.; Pan, H. Study of planning and design of hybrid AC/DC micro-grid. *J. Hefei Univ. Technol. Nat. Sci.* **2015**, *38*, 166–170.
3. Chen, J.; Chen, X.; Feng, Z.Y.; Gong, C.Y.; Yan, Y.G. A control strategy of seamless transfer between grid-connected and islanding operation for microgrid. *Proc. CSEE* **2014**, *34*, 3089–3097.

4. Chen, J.; Niu, B.W.; Zhang, J.W.; Chen, X.; Gong, C.Y. Hybrid control strategy for the seamless transfer of microgrids. *Proc. CSEE* **2015**, *35*, 4379–4387.
5. Chen, X.; Ji, Q.H.; Liu, F. Smooth transferring control method of microgrids based on master-slave configuration. *Trans. China Electrotech. Soc.* **2014**, *29*, 163–170.
6. Wang, C.S.; Li, X.L.; Guo, L.; Li, Y.W. A seamless operation mode transition control strategy for a microgrid based on master-slave control. *Sci. China Technol. Sci.* **2012**, *55*, 1644–1654. [CrossRef]
7. Qiu, L.; Xu, L.; Zheng, Z.D.; Li, Y.D.; Zheng, Z.X. Control method of microgrid seamless switching. *Trans. China Electrotech. Soc.* **2014**, *29*, 171–176.
8. Zheng, T.W.; Chen, L.J.; Mei, S.W. Smooth transition control in a master-slave micro-grid considering timing-sequence-coordination. *Electr. Energy Manag. Technol.* **2014**, *10*, 44–49.
9. Bi, D.Q.; Zhou, W.; Dai, Y.X.; Li, X.G. Control strategies of seamless switching for energy storage converter in hybrid AC/DC microgrid. *Autom. Electr. Power Syst.* **2016**, *40*, 84–89.
10. Zeng, L.; Jinjun, L. A three-phase inverter control method which can realize smooth switching of distributed power generation system is presented. *Trans. China Electrotech. Soc.* **2011**, *26*, 52–61.
11. Shudong, W.; Wei, D.; Huanyu, W. Research on parallel/Off-grid switching Technology of Microgrid based on improved nonlinear Sag Control. *Electr. Meas. Instrum.* **2018**, *55*, 112–118.
12. Driesen, J.; Katiraei, F. Design for Distributed Energy Resources. *IEEE Power Energy Mag.* **2008**, *6*, 30–40.
13. Wei, T. Research on Operation Control Strategy of Hybrid Microgrid. Ph.D. Thesis, China University of Mining and Technology, Xuzhou, China, 2020.
14. Han, G. Research on Control Strategy of ACDC Bidirectional Power Converter in ACDC Hybrid Microgrid. Ph.D. Thesis, Taiyuan University of Technology, Taiyuan, China, 2019.
15. Wenchao, X.; Yongqiang, Z.; Ruihua, X. Power Hierarchical Control of AC-DC Hybrid Microgrid with Multiple interconnected converters Running side-by-side. *Shaanxi Electr. Power* **2016**, *44*, 9–13+56.
16. Yuan, F.; Yi, W.; Xiangyu, Z. Analysis and integrated control of inertia and primary frequency regulation for variable speed wind turbines. *Proc. CSEE* **2014**, *34*, 4706–4716.